ACS OMEGA

Open Access

http://pubs.acs.org/journal/acsodf

Article

Synthesis and Characterization of Naproxen Intercalated Zinc Oxide Stacked Nanosheets for Enhanced Hepatoprotective Potential

Muhammad Saleem Mughal, Bilal Akram,* Bilal Ahmad Khan,* Tafail Akbar Mughal, Sulaiman Sulaiman, Omar H. Abd-Elkader, Shaban R. M. Sayed, Mahmoud A. A. Ibrahim,* and Ahmed M. Sidky

Cite This: *ACS Omega* 2024, 9, 22979−22989

Read Online

ACCESS | Metrics & More | Article Recommendations

ABSTRACT: Liver diseases pose a significant global health burden, with limited therapeutic options for chronic cases. Zinc oxide (ZnO) nanomaterials have emerged as promising candidates for hepatoprotection due to their antioxidant, anti-inflammatory, and regenerative properties. However, their potential remains hampered by insufficient drug loading and controlled release. The current study explores the intercalation of Naproxen (Nx), a potent anti-inflammatory and analgesic drug, within ZnO stacked nanosheets (SNSs) to address these limitations. Herein, an easy and solution-based synthesis of novel Nx intercalated ZnO SNSs was established. The obtained Nx intercalated ZnO SNSs were encapsulated with poly(vinyl acetate) (PVA) to make them biocompatible. The synthesized biocomposite was characterized using X-ray diffraction (XRD), scanning electron microscopy (SEM), and Fourier transform infrared spectroscopy (FTIR), which confirm the successful synthesis and intercalation of Nx within the ZnO SNSs. The obtained outcomes showed that the configuration of ZnO nanosheets was altered when Nx was introduced, resulting in a more organized stacking pattern. An *in vivo* investigation of mice liver cells unveiled that the Nx intercalated ZnO SNss had increased hepatoprotective properties. The study's results provide valuable insights into using Nx intercalated ZnO SNss for targeted drug delivery and improved treatment effectiveness, particularly for liver-related illnesses.

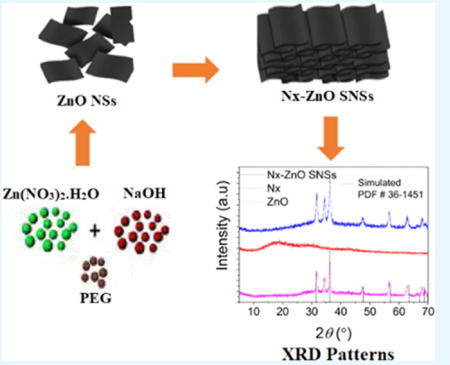

1. INTRODUCTION

Nanosheets represent a category of two-dimensional nanomaterials characterized by their exceedingly small thickness, typically measured in nanometers and lateral dimensions spanning from submicrons to micrometers.[1,2] These nanosheets are anticipated to serve as a crucial link between the quantum realm of zero- or one-dimensional nanomaterials and the three-dimensional expanse of macroscopic bulk materials.[3,4] Significantly, their primary distinguishing characteristic is their substantial specific surface area, which renders them exceptionally auspicious alternatives for an extensive array of applications, especially in the domains of biomedical applications.[5−9]

Various types of nanosheets composed of oxidized substrates, such as silicate layers or metal oxides, have been successfully synthesized. Numerous strategies were devised to produce nanosheets through various synthetic methods. These include mechanical exfoliation,[10] electrochemical Li-intercalation and exfoliation,[11,12] direct sonication in solvents,[13] wet chemical synthesis,[14] and chemical vapor deposition (CVD),[15] among others. However, many of these methods entail multistep processes for hybrid nanosheet fabrication, posing challenges in controlling the distribution of components within the nanosheets.

Nevertheless, there is a paucity of reports on the fabrication of two-dimensional nanomaterials using an easy low-temperature solution-based strategy.[16−19] The easy and solution-based synthesis approach typically involves straightforward procedures using readily available chemicals and equipment. This accessibility allows researchers with varying levels of expertise and resources to employ these methods, democratizing the field of nanoparticle synthesis. Such synthetic approaches are often easily scalable, enabling the production of nanoparticles in larger quantities without significant increases in complexity or cost.[20,21]

Zinc oxide (ZnO) is a versatile semiconductor material characterized by a wide band gap of 3.37 electronvolts (eV) and a substantial excitation binding energy of 60 millivolts

Received: March 9, 2024
Revised: April 16, 2024
Accepted: April 29, 2024
Published: May 13, 2024

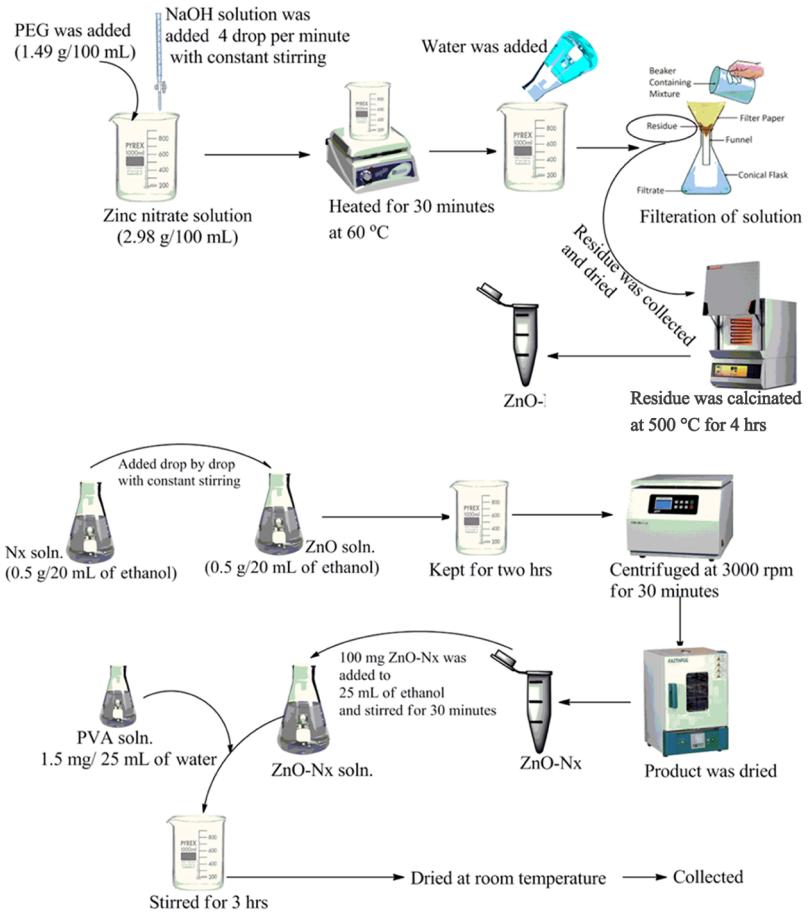

Figure 1. Pictorial representation of the synthetic strategy of Nx-P.

(mV) at room temperature.[22−24] While initially employed in industrial manufacturing, the applications of ZnO nanomaterials have significantly expanded into the realm of biology.[24,25] It is widely recognized that zinc, an essential trace element, is prevalent in various body tissues, including the brain, muscle, bone, and skin. Zinc plays a pivotal role in numerous enzyme systems, influencing metabolic processes, protein and nucleic acid synthesis, hematopoiesis, and neurogenesis.[26−29] Nano-sized ZnO particles, due to their diminutive size, facilitate enhanced absorption by the human body, making nano-ZnO a common food additive. Furthermore, it is essential to note that the United States Food and Drug Administration (FDA) designates ZnO as Generally Recognized As Safe "GRAS."[30] Given these characteristics, ZnO-based nanomaterials have garnered increased attention in biomedical applications. In comparison to other metal oxide nanomaterials, ZnO-based counterparts are not only cost-effective but also relatively less toxic.[31,32] Consequently, they have demonstrated remarkable potential in diverse biomedical applications, including anticancer therapies, drug delivery systems, antibacterial agents, diabetes treatment, anti-inflammatory interventions, wound healing, and bioimaging.[23,33,34]

To unlock the full biomedical potential of ZnO-based nanomaterials, their capabilities can be augmented by coupling them with biomolecules, including various antibiotic medications.[35] In nature, interactions between biomolecular pairs with distinct high affinities are widespread. When one of these biomolecular entities conjugates with the nanoparticles, the resulting biofunctional nanomaterials can selectively adhere to the complementary biomolecular entity.[36] This principle has underpinned the development of numerous applications employing biofunctional nanoparticles, including but not limited to pathogen detection, protein purification, and toxin removal.[37,38]

Naproxen (Nx), a nonsteroidal anti-inflammatory drug, is widely used for its analgesic and anti-inflammatory properties.[39] However, its clinical use is limited due to the potential hepatotoxicity associated with its prolonged or high-dose administration. Hepatotoxicity, characterized by liver injury and dysfunction, is a significant concern in the therapeutic use of Nx.[40] Therefore, there is a need for strategies to enhance the hepatoprotective potential of Nx while minimizing its adverse effects.

Commonly employed techniques for modifying the surface of ZnO nanoparticles involve treatments such as silanization, amine coating, and the use of polymeric agents like poly(vinyl alcohol) (PVA) and chitosan.[41] These methods are applied to address solubility challenges.[42] By employing these coating agents, the dispersion of nanoparticles in biological fluids can be significantly enhanced, thereby improving their antimicrobial effectiveness. Moreover, these coatings protect ZnO nanoparticles, rendering them suitable for biolabeling applications.[43]

A hydrophilic cationic polymer called poly(vinyl alcohol) (PVA) finds extensive applications in various biological contexts, including antimicrobial properties and as carriers for drugs. PVA enhances the colloidal stability of nanoparticles, promoting cellular internalization through electrostatic inter-

https://doi.org/10.1021/acsomega.4c02319
ACS Omega 2024, 9, 22979−22989

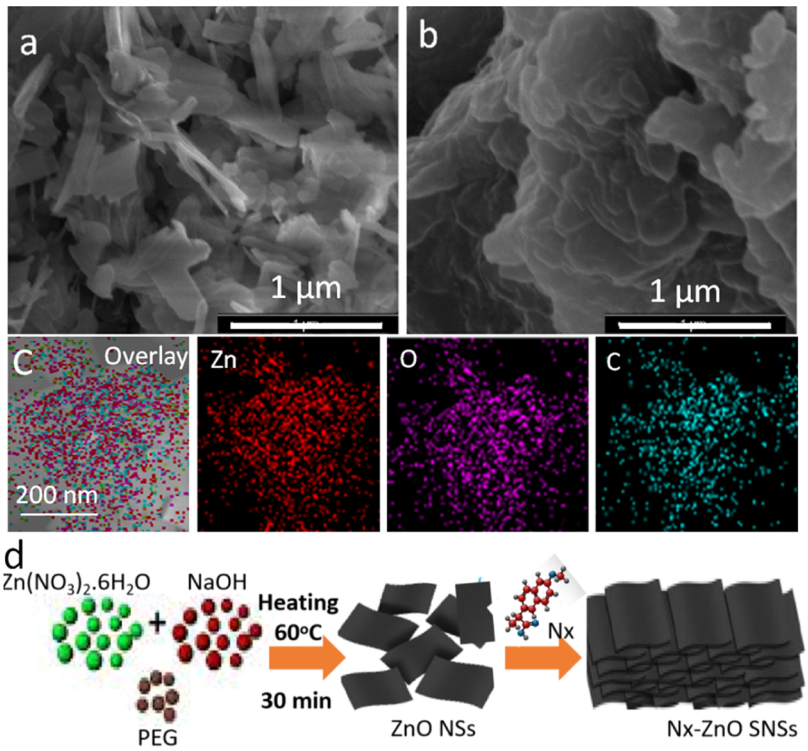

Figure 2. (a) SEM image of ZnO NSs, (b) SEM image of Nx-ZnO SNSs, (c) EDX elemental mapping of Nx-ZnO SNSs, and (d) scheme of the formation of Nx-ZnO SNSs.

actions with membrane proteins.[44,45] Studies have shown that modifying ZnO with PVA can improve their performance by regulating nucleation based on molecular weight and concentration. Additionally, the physical properties of ZnO nanoparticles undergo variation with PVA coating, leading to enhanced antibacterial activity.[46] This suggests that PVA can mitigate nanoparticle solubility issues through surface modification.

In this respect, the current work was devoted to developing an easy low-temperature solution-based approach to synthesize Nx-based ZnO NSs-based biocomposite with enhanced biological potential. A two-step method was employed to obtain bioconjugated stacked ZnO nanosheets. First, a coprecipitation method was adopted to obtain ZnO NSs at low-temperature, followed by the dropwise addition of Nx. The introduced Nx not only enhanced the biological potential but also led to the stacking of preformed ZnO nanosheets. By employing suitable characterization methods, the structural and physicochemical properties of the intercalated nanosheets were investigated. Furthermore, an *in vivo* investigation of mice liver cells was demonstrated to provide insights into the potential of this nanomaterial-based approach for hepatoprotection. The findings of this study could contribute to the development of safer and more effective therapeutic interventions for liver diseases associated with inflammation and oxidative stress.

2. MATERIALS AND METHODS

Zinc nitrate $(ZnNO_3)_2{\cdot}6H_2O$, sodium hydroxide (NaOH), poly(ethylene glycol) (PEG, 6000), naproxen (Nx), poly(vinyl acetate) (PVA, 89−98,000, 99% hydrolyzed), carbon tetrachloride (CCl_4), and ethanol were purchased from Sigma-Aldrich. Deionized water was used throughout the experiment.

2.1. Synthesis of Nanomaterials. *2.1.1. Step 1. Synthesis of Zinc Oxide Nanoparticles.* As the precursor salt, $Zn(NO_3)_2{\cdot}6H_2O$ was reduced using NaOH to produce ZnO NSs. An aqueous solution of 100 mM (2.98 g/100 mL) $ZnNO_3$ was prepared. PEG was then dissolved in the $Zn(NO_3)_2$ solution, where the amount of the PEG was equal to half of $ZnNO_3$ (i.e., 1.49 g/100 mL). An aqueous solution of 100 mM (0.5 g/125 mL) of the NaOH was also prepared in water.

100 mM solution of NaOH was added to the $Zn(NO_3)_2$ solution by four drops per minute with a constant stirring speed until the solution turned basic with a pH of 10. The solution was then heated at 60 °C for 30 min. Afterward, enough water was added to the solution to turn it neutral. The solution was finally filtered, and residue was collected. The residue was dried and calcinated at 500 °C for 4 h.

2.1.2. Step 2. Synthesis of PVA Capped Nx Intercalated ZnO SNSs (Nx-P). The solution of ZnO and Nx was prepared in a fixed ratio (0.025 g/mL) in 20 mL of ethanol. The solution of Nx drug was added to the ZnO solution drop by drop with a constant stirring speed. The solution was kept for 2 h poststirring, then centrifuged at the rate of 3000 rpm for 30 min. The product was dried and collected. The loaded amount of drug was estimated gravimetrically, and it comes out to be 0.69 g/g of the ZnO NSs.

The solution of ZnO-Nx SNSs was prepared in ethanol at a fixed ratio (4 mg/mL) and stirred for 30 min. The solution of PVA was prepared (0.06 mg/mL) in 25 mL of water. The PVA solution was added to the ZnO-Nx SNSs solution. The obtained mixture was stirred for a further 3 h, and the product was dried at room temperature. The PVA capped Nx intercalated ZnO SNSs are named as Nx-P hereafter. The pictorial representation of a brief experimental procedure is illustrated in Figure 1.

https://doi.org/10.1021/acsomega.4c02319
ACS Omega 2024, 9, 22979−22989

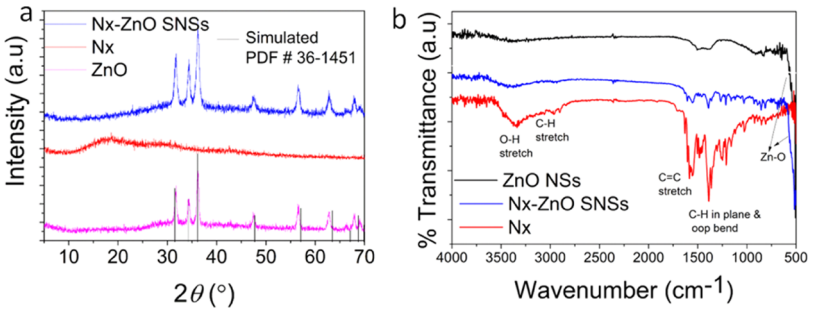

Figure 3. (a) XRD patterns and (b) FTIR spectrum of ZnO NSs, Nx, and Nx-ZnO SNSs.

2.2. Characterization of ZnO-Nx SNSs. The synthesized materials were characterized using a UV−vis spectrometer (PerkinElmer, Lambda 25), Fourier transform infrared spectroscopy (FTIR) (JASCO FT/IR-6600), X-ray diffraction (XRD) analysis (D8 advanced Bruker X-ray diffractometer) (Bruker Germany), and scanning electron microscopy (SEM).

2.3. Experimental Animals and Dose Preparation. This study was restricted to the group and investigation of data from 30 male Swiss albino mice *Mus musculus domesticus* (average age 8 weeks; body mass 35 g) taken from the National Institute of Health (NIH), Islamabad. Animals were housed in various polypropylene cages according to their treatment regimens and given access to refined water and standard laboratory pellets as needed. The animal home was maintained at 22 ± 2 °C with a cycle of 12 h of light and 12 h of darkness. They were lodged together for 7 days before the beginning of the trial and were categorized into six groups for the hepatoprotective activity of sample-1 in a whimsical way; **Group I:** control group; these animals did not get any sort of treatment. Twenty-five animals got a single intraperitoneal (IP) dosage of CCl_4 (0.4 mL/kg body weight) for stimulation of disease. Next to the CCl_4 induction, animals that caused disease were further categorized into four groups: **Group II:** CCl_4 treated group; **Group III:** diseased animals that were treated with oral daily dose (via 18-gauge oral feeding needle) of CCl_4 + Nx (400 mg/kg) for 12 consecutive days; **Group IV:** diseased animals that were treated with an oral daily dose of CCl_4 + ZnO (400 mg/kg) for 12 consecutive days; **Group V**: diseased animals that were treated with CCl_4 + ZnO-Nx (400 mg/kg) for 12 consecutive days; and **Group VI:** diseased animals that were treated with oral daily dose of CCl_4 + Nx-P (400 mg/kg) for 12 consecutive days. The hepatoprotective activity was assessed by comparing the levels of various biochemical components in plasma and compared with the hepatoprotective effect of CCl_4. Enzymes and protein contents were extracted and estimated by a method mentioned by Mughal et al.[47]

2.4. Estimation of Biochemical Components in Liver. The level of total protein, total bilirubin, AST, ALT, ALP, MDA, GSH, Catalase, and LDH in the saline extract of plasma were assessed by the method designated by Mughal et al.[47]

2.5. Statistical Analysis. All arithmetics calculations were carried out using GraphPad Prism version 5. Each value was expressed as mean ± SEM. A one-way analysis of variance (ANOVA) with the Bonferroni test was employed to assess the arithmetical variation among the various groups. At $p \leq 0.05$, $p \leq 0.01$, and $p \leq 0.001$, values were deemed statistically significant.

3. RESULTS AND DISCUSSION

3.1. ZnO NSs and Nx-ZnO SNSs Characterization. The structural features and stacked nature of ZnO NSs were investigated using electron microscopy analysis. The SEM image in Figure 2a conspicuously unveiled that the free-standing ZnO NSs have a nonuniform distribution of length and width. Upon adding Nx into the synthesized ZnO NSs, the stacking of ZnO NSs was reformed into highly ordered stacked arrangements, as displayed in Figure 2b. Elemental mapping through energy dispersive X-ray (EDX, Figure 2c) of Nx-ZnO SNSs revealed that all of the elements are uniformly distributed in the whole structure. The formation scheme of Nx-ZnO SNSs is given in Figure 2d. The ordered stacking of ZnO NSs in the presence of Nx might be due to various interactions such as van der Waals forces, hydrogen bonding, or electrostatic interactions. These interactions may develop upon the addition of Nx, which hinders the mobility of ZnO NSs, limiting their ability to move freely and aggregate randomly. This could promote a more ordered arrangement of the NSs. Moreover, the interaction between the electron-rich regions of Nx molecules and the electron-deficient regions on the surface of ZnO NSs could induce charge transfer effects, influencing the assembly of the nanosheets into ordered structures.

In order to examine the compositional purity and effective formation of the biocomposite, XRD analysis was implemented. As shown in Figure 3a, sharp peaks were observed in the XRD pattern of the synthesized ZnO SNSs, confirming their well-crystalline structure. The acquired pattern exhibits adequate indexing with JCPDS No. 36-1451, denoting the hexagonal phase of ZnO. An analysis of the XRD patterns of the constituent elements revealed that Nx lacks distinct peaks and exhibits an amorphous structure. The Nx addition does not affect the XRD pattern of SNSs.

The functional characteristics and bond vibrations of the ZnO NSs, Nx, and Nx-ZnO SNSs were analyzed utilizing FTIR spectroscopy. FTIR spectrum of the Nx-ZnO SNSs and their constituent elements are illustrated in Figure 3b.

Due to stretching vibrations of the Zn−O bonds, the characteristic peak of ZnO NSs was found at 555 cm^{-1}, indicating the hexagonal phase of ZnO NSs.[4] The distinct bands observed in the FTIR spectrum of Nx were located at 3120, 1720, 1600, 1390, 1177, 854, and 673 cm^{-1}, which were assigned to the aliphatic chain's C−H vibrations, C═O, C═C, CH_3, C−H in-plane, C−H out-of-plane, and C−C (ring bending), respectively. At 3350 cm^{-1}, the O−H stretching vibrations were responsible for the characteristic bands.[48,49] Successful intercalation of Nx into ZnO NSs was confirmed by the appearance of Nx characteristic bands in the Nx-ZnO SNSs.

https://doi.org/10.1021/acsomega.4c02319
ACS Omega 2024, 9, 22979−22989

The optical properties of synthesized Nx-ZnO SNSs were investigated using UV−vis spectroscopy. On the UV−vis plots shown in Figure 4, the intercalation of the Nx shifted the

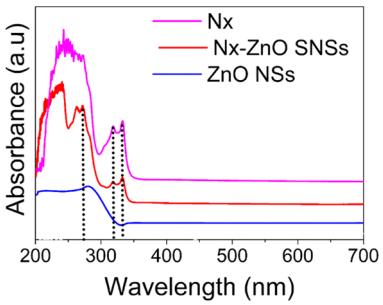

Figure 4. UV−vis spectra of ZnO NSs, Nx, and Nx-ZnO SNSs.

absorption toward the red end as compared to sole ZnO NSs. The ZnO has a band at 272 nm and Nx has two bands at 312 and 333 nm. Moreover, the characteristic absorption bands of both Nx and ZnO can be clearly seen in Nx-ZnO SNSs, further evidencing the successful formation of biocomposite.

In order to make the Nx intercalated ZnO NSs more biocompatible, the Nx-ZnO SNSs were coated with PVA. The introduced PVA encapsulated the SNSs into compact structures, as indicated in the SEM image (Figure 5). The XRD pattern of PVA-encapsulated SNSs proclaimed that the ZnO phase and crystalline nature remain well intact even after encapsulation (Figure 5b). The capping of PVA onto Nx-ZnO SNSs enhances biocompatibility and provides additional advantages, one of which could be relevant to the applicability of PVA as a stabilizing agent. It acts as a barrier to prevent the oxidation of Nx. By capping Nx-ZnO SNSs with PVA, a protective layer is formed around the SNSs, shielding them from oxidation and preserving their integrity and functionality over time. PVA improves the dispersibility of nanostructures in various solvents and matrices. The hydrophilic nature of PVA allows for better dispersion in aqueous solutions, which is essential for applications such as drug delivery, biological labeling, and nanocomposite synthesis. Improved dispersion ensures homogeneous distribution and enhances interaction with other materials or biological systems.

3.2. *In vivo* Hepatoprotective Activity. The liver metabolizes substances that enter the body and detoxifies them. Hepatic damage could happen throughout this process.[50] The effects on the liver are positioned as the primary toxicological consequences associated with a variety of illnesses.[51] Toxic substances cause oxidative damage in the hepatocytes.[52] There are numerous medications available to treat liver disorders.[53] Hepatoprotective activity describes a substance's or compound's capacity to defend the liver against harm and advance its general health.[54,55] Newly synthesized biocompatible Nx-ZnO SNSs were explored for their potential hepatoprotective effects.

3.2.1. Effect on Alanine Transaminase (ALT). Intraperitoneal administration of CCl_4 (0.4 mL/kg body weight) caused a significant upsurge (153.2 ± 5.08 U/L) in the level of ALT as compared to the control (42.4 ± 1.93 U/L). High significant reversal was observed in mice groups when CCl_4 was given in combination with Nx (61.74 ± 2.96 U/L), ZnO (65.4 ± 5.93 U/L), ZnO-Nx (59 ± 4.6 U/L), and Nx-P (57.4 ± 6.06 U/L) as compared to CCl_4 (153.2 ± 5.08 U/L) (Figure 6A).

3.2.2. Effect on Aspartate Aminotransferase (AST). Intraperitoneal administration of CCl_4 (0.4 mL/kg body weight) caused a significant upsurge (462.2 ± 4.20 U/L) in the level of AST as compared to the control (84.2 ± 1.49 U/L). A highly significant reversal was observed in mice groups when CCl_4 was given in combination with Nx (218.4 ± 11.00 U/L), ZnO (265.4 ± 18.89 U/L), ZnO-Nx (228 ± 7.50 U/L), and Nx-P (168.4 ± 10.73 U/L) as compared to CCl_4 (462.2 ± 4.20 U/L) (Figure 6B).

3.2.3. Effect on Alkaline Phosphatase (ALP). Intraperitoneal administration of CCl_4 (0.4 mL/kg body weight) caused a significant upsurge (303 ± 15.5 U/L) in the level of ALP as compared to control (111.4 ± 3.61 U/L). Upon the introduction of CCl_4 in combination with Nx, ZnO-Nx, and Nx-P, a highly significant increase of ALP levels was observed in mice groups with values of 213.8 ± 3.68, 196 ± 10.90 and 195.6 ± 11.4 U/L, respectively, as compared to CCl_4 (303 ± 15.5 U/L). In addition, a significant reversal was noticed in mice groups that received CCl_4 in combination with ZnO (239.8 ± 15.5 U/L) (Figure 6C).

3.2.4. Effect on Lactate Dehydrogenase (LDH). Intraperitoneal administration of CCl_4 (0.4 mL/kg body weight) caused a significant upsurge (995 ± 64.94 U/L) in the level of LDH as compared to the control (329.9 ± 19.38 U/L). As seen with ALT, AST, and ALP, a significant reversal was noticed in mice groups when CCl_4 was given in combination with ZnO-Nx (588.2 ± 41.96 U/L) and Nx-P (583.8 ± 60.99 U/L) as compared to CCl_4 (995 ± 64.94 U/L). Also, a significant reversal was observed in mice groups when CCl_4 was given in combination with ZnO (626.4 ± 53.88 U/L). No significant change was observed in mice groups when CCl_4 was given in combination with Nx (Figure 6D).

3.2.5. Effect on Liver Malondialdehyde (MDA). When CCl_4 admitted intraperitonealy (0.4 mL/kg body weight), a significant upsurge (652.2 ± 20.2 mmol/g liver) in the level

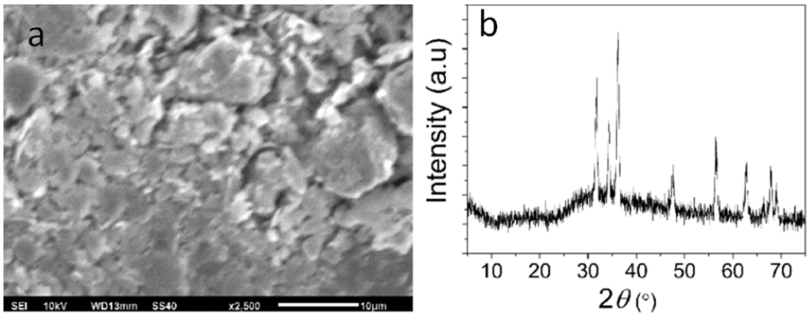

Figure 5. (a) SEM image and (b) XRD pattern of PVA-coated Nx-ZnO SNSs.

https://doi.org/10.1021/acsomega.4c02319
ACS Omega 2024, 9, 22979−22989

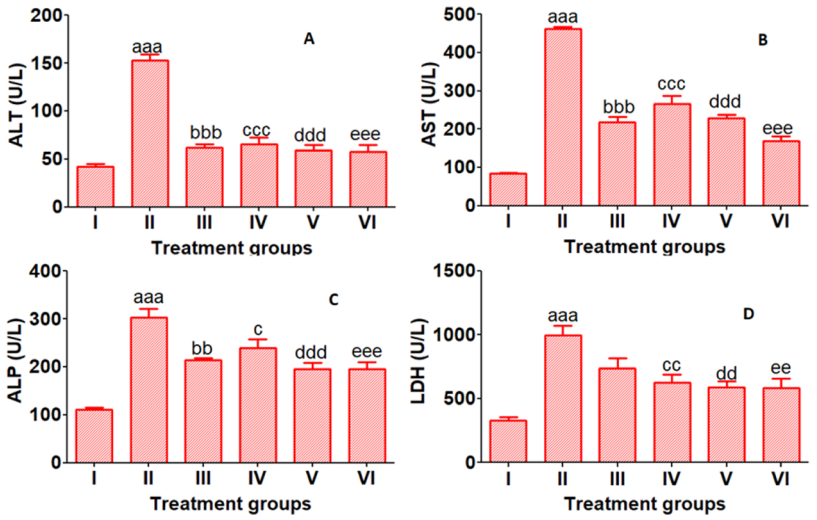

Figure 6. Analysis of enzymes A (ALT), B (AST), C (ALP), and D (LDH) in the liver of Balb C mice I: Control; II: CCl_4; III: CCl_4 + Nx; IV: CCl_4 + ZnO; V: CCl_4 + ZnO-Nx; VI: CCl_4 + Nx-P. Key: [a]depicts variance between I and II. [b]depicts variance between II and III. [c]depicts variance between II and IV. [d]depicts variance between II and V. [e]depicts variance between II and VI. Each bar represents the mean value of five replicates and SEM. Arithmetical icons: c = $p \leq 0.05$; bb,cc,dd,ee = $p \leq 0.01$; aaa, bbb, ccc, ddd, eee = $p \leq 0.001$.

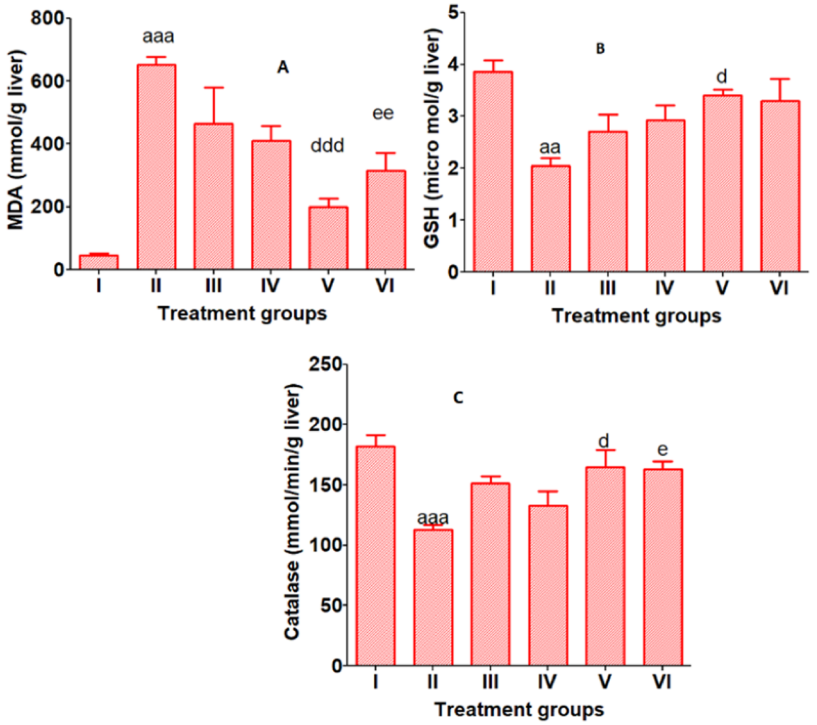

Figure 7. Analysis of enzymes A (MDA), B (GSH) and C (Catalase) in the liver of Balb C mice I: Control; II: CCl_4; III: CCl_4 + Nx; IV: CCl_4 + ZnO; V: CCl_4 + ZnO-Nx; VI: CCl_4 + Nx-P. Key: [a]depicts variance between I and II. [b]depicts variance between II and III. [c]depicts variance between II and IV. [d]depicts variance between II and V. [e]depicts variance between II and VI. Each bar represents the mean value of five replicates and SEM. Arithmetical icons: d,e = $p \leq 0.05$; aa,ee = $p \leq 0.01$; aaa,ddd = $p \leq 0.001$.

of MDA was noticed as compared to the control (46.2 ± 4.45 mmol/g liver). A highly significant reduction in MDA levels was observed in mice groups when CCl_4 was given in combination with ZnO-Nx (200.6 ± 22.98 mmol/g liver) and Nx-P (315.6 ± 48.11 mmol/g liver) as compared to CCl_4 (652.2 ± 20.2 mmol/g liver). However, no significant change was observed in mice groups when CCl_4 was given in combination with either Nx or ZnO (Figure 7A).

3.2.6. Effect on Glutathione (GSH). Intraperitoneal administration of CCl_4 (0.4 mL/kg body weight) gave rise to a significant reduction in the levels of GSH (2.04 ± 0.12 μmol/g liver) as compared to the control (3.85 ± 0.18 μmol/g liver). A considerable reversal was observed in mice groups when CCl_4 was given in combination with ZnO-Nx (3.4 ± 0.09 μmol/g liver) compared to CCl_4 (2.04 ± 0.12 μmol/g liver). When Nx-P, Nx, and ZnO were given in combination with CCl_4, no change was observed in mice groups (Figure 7B).

3.2.7. Effect on Catalase. Intraperitoneal administration of CCl_4 (0.4 mL/kg body weight) caused a significant depression

https://doi.org/10.1021/acsomega.4c02319
ACS Omega 2024, 9, 22979−22989

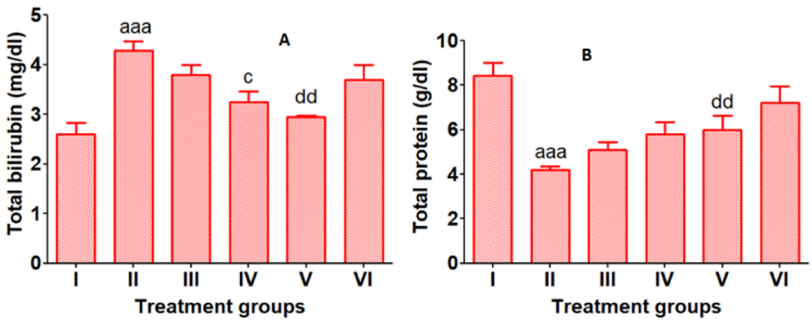

Figure 8. Analyses of A (total bilirubin) and B (total protein) in the liver of Balb C mice I: Control; II: CCl_4; III: CCl_4 + Nx; IV: CCl_4 + ZnO; V: CCl_4 + ZnO-Nx; VI: CCl_4 + Nx-P. Key: [a]depicts variance between I and II. [b]depicts variance between II and III. [c]depicts variance between II and IV. [d]depicts variance between II and V. [e]depicts variance between II and VI. Each bar represents the mean value of five replicates and SEM. Arithmetical icons: dd = $p \leq 0.01$; aaa = $p \leq 0.001$.

(112.8 ± 3.44 mmol/min/g liver) in the level of Catalase as compared to the control (182 ± 7.76 mmol/min/g liver). A sharp increase in Catalase levels was observed only in mice groups treated with CCl_4 in combination with ZnO-Nx (164.6 ± 12.16 mmol/min/g liver) and Nx-P (163 ± 5.43 mmol/min/g liver) as compared to CCl_4 (112.8 ± 3.44 mmol/min/g liver). However, when Nx and ZnO were given in combination with CCl_4, no significant changes were observed in mice groups (Figure 7C).

3.2.8. Effect on Total bilirubin. Intraperitoneal administration of CCl_4 (0.4 mL/kg body weight) led to a significant depression (4.28 ± 1.5 mg/dL) in the level of Total bilirubin as compared to the control (2.6 ± 0.18 mg/dL). A highly significant reversal effect was observed in mice groups when CCl_4 was given in combination with ZnO-Nx (2.94 ± 0.03 mg/dL) compared to the CCl_4 (4.28 ± 1.5 mg/dL). A similar effect was observed in mice groups when CCl_4 was given in combination with ZnO (3.24 ± 0.18 mg/dL). When Nx-P and Nx were given in combination with CCl_4, no change was observed in mice groups (Figure 8A).

3.2.9. Effect on Total Protein. Intraperitoneal administration of CCl_4 (0.4 mL/kg body weight) caused a significant depression (4.18 ± 0.15 g/dL) in the level of total protein as compared to the control (8.42 ± 0.49 g/dL). Exclusively, when CCl_4 was given in combination with ZnO-Nx, a highly significant reversal effect was observed in mice groups, i.e., (6.0 ± 0.53 g/dl) as compared to the CCl_4 (4.18 ± 0.15 g/dL). Nonetheless, no significant changes in the levels of total protein were observed when Nx-P, ZnO, and Nx were given in combination with CCl_4 (Figure 8B).

3.3. CCl_4-Induced Hepatotoxicity and Potential Preventive Measures. Dry cleaning agents, refrigerants, and solvents for oils and fats are all used for CCl_4. The kidneys and liver are harmed when CCl_4 is inhaled. Additionally, CCl_4 is a carcinogen for humans.[56] The liver serves as our body's primary detoxifying organ,[57] which is why most toxicological issues are related to it.[58] Hepatotoxicants cause oxidative damage to liver cells.[59] This shows the importance of researching CCl_4-induced hepatotoxicity and potential preventive measures. The administration of a single CCl_4 dose to Balb C mice has led to a highly significant rise in plasma levels of ALT, AST, ALP, LDH, and MDA. Moreover, it caused a sharp decline in the level of GSH and Catalase in comparison to control and Nx, ZnO, and nanoformulations (i.e., ZnO-Nx and Nx-P).[47] When the combination of CCl_4 and Nx, ZnO, and nanoformulations (i.e., ZnO-Nx and Nx-P) was given, a highly significant reversal in ALT and AST levels in plasma was observed. A highly significant decrease in the level of ALP was found when the combinations of CCl_4 and ZnO-Nx, Nx-P and Nx were given, as well as a substantial decrease in the level of ALP was observed when ZnO was given in combination with CCl_4. When the combination of CCl_4, ZnO, and nanoformulations (i.e., ZnO-Nx, Nx-P) was given to the mice, a highly significant reversal in the level of LDH in plasma was found. No change in the level of LDH was found when Nx combination with CCl_4 was given to the mice that may support our hypothesis of the importance of ZnO SNSs combined with Nx as hepatoprotective compounds. When the combination of CCl_4 and nanoformulations (i.e., ZnO-Nx, Nx-P) was given, a significant reversal in the level of MDA in plasma was observed. No change in the level of MDA was observed when Nx and ZnO combination with CCl_4 was given to the mice, which, again, support the importance of having Nx and ZnO SNSs combined together as a potential treatment. When the combination of CCl_4 and ZnO-Nx was given, significant reversal in the level of GSH in plasma was observed. While no change in the level of GSH was observed when Nx, Nx-P, and ZnO combination with CCl_4 was given to the mice. When the combination of CCl_4 and ZnO-Nx was given, a highly significant reversal in the level of Catalase in plasma was observed. Furthermore, a significant reversal in the level of Catalase in plasma was observed with Nx-P; however, no change in the level of Catalase was observed when Nx and ZnO combination with CCl_4 was given to the mice.

CCl_4 intraperitoneal administration produced a highly significant drop in hepatic total protein, and a surge in the total bilirubin was related to control. According to Benahmed et al.,[60] when the combination of CCl_4 and ZnO-Nx was given, a highly significant reversal in the total bilirubin level in plasma was observed. Moreover, when the combination of CCl_4 and ZnO was given, a significant reversal in the total bilirubin level in plasma was observed. In contrast, no change in the total bilirubin level was observed when Nx and Nx-P combination with CCl_4 was given to the mice. When the combination of CCl_4 and ZnO-Nx was given, a highly significant reversal in the total protein level in plasma was observed. No alteration in the level of total protein was observed when ZnO, Nx, and Nx-P combination with CCl_4 was given to the mice. The obtained findings demonstrated the effectiveness of freshly synthesized nanoformulations (i.e., ZnO-Nx, Nx-P) in treating CCl_4-induced hepatotoxicity.

Hematoxylin and eosin (H&E) staining is a common histological technique used to evaluate tissue morphology and identify cellular structures under a microscope. H&E staining

https://doi.org/10.1021/acsomega.4c02319
ACS Omega 2024, 9, 22979−22989

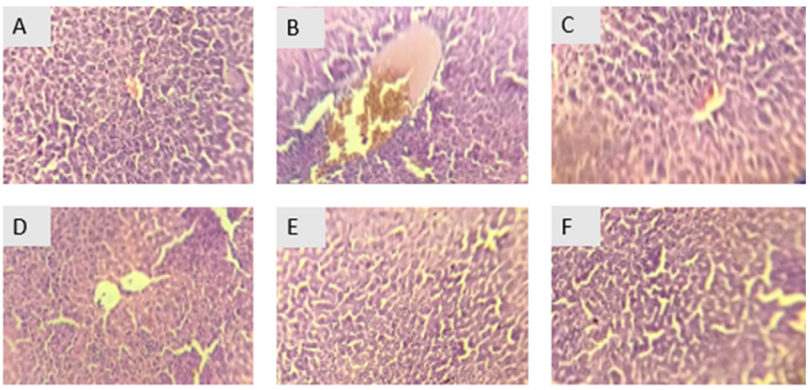

Figure 9. Histopathology of liver. (A) Control; (B) CCl_4; (C) CCl_4 + Nx; (D) CCl_4 + ZnO; (E) CCl_4 + ZnO-Nx; (F) CCl_4 + Nx-P.

was applied to assess the toxicity of various materials whose microscopic images are shown in Figure 9.

3.4. Discussion on the Enhanced Liver Protective Potential of Nx Intercalated ZnO SNSs. The enhancement of liver protective potential by Nx (a nonsteroidal anti-inflammatory drug) intercalation into ZnO SNSs involves several factors, including the following:

3.4.1. Synergistic Effects. ZnO SNSs are known for their potential in various biomedical applications due to their unique properties, such as high surface area, tenable morphology, and biocompatibility. When combined with Nx, the synergistic effects of the two materials may enhance their liver protective potential. Nx's anti-inflammatory properties can complement ZnO's inherent properties, resulting in a more potent protective effect against liver damage. A plausible explanation for the synergistic hepatoprotective effect is also addressed. ZnO nanosheets may possess inherent hepatoprotective properties by scavenging reactive oxygen species (ROS) and modulating cellular oxidative stress responses. When combined with Nx, these effects could be amplified due to the synergistic action of both agents. The intercalation of Nx with ZnO NSs may enhance the bioavailability of the drug by overcoming barriers such as poor solubility or rapid metabolism, resulting in higher concentrations of Nx at the target site and improved hepatoprotective effects.

3.4.2. Drug Delivery Mechanisms. The insertion of Nx into ZnO SNSs could facilitate controlled drug delivery to the liver. ZnO SNSs can serve as carriers for Nx, allowing for sustained release and targeted delivery to the liver, where it can exert its protective effects more efficiently. This controlled release mechanism could enhance the bioavailability and efficacy of Nx, leading to improved liver protection.

3.4.3. Reduced Toxicity. ZnO SNSs have been shown to possess intrinsic antioxidant properties and low cytotoxicity, making them suitable candidates for biomedical applications. By encapsulating Nx within ZnO SNSs, the potential toxic effects of Nx could be mitigated, thereby reducing the risk of adverse side effects on the liver and other organs. This encapsulation may also enhance the stability of Nx, preventing its degradation and ensuring sustained therapeutic activity.

3.4.4. Cellular Interactions. The unique structure of ZnO SNSs allows for interactions with biological systems at the cellular level. The insertion of Nx into ZnO SNSs could facilitate interactions with liver cells, such as hepatocytes and Kupffer cells, leading to modulation of inflammatory responses and promotion of cell survival pathways. These cellular interactions could contribute to the enhanced liver protective potential observed with Nx-inserted ZnO SNSs.

Overall, the intercalation of Nx into ZnO NSs enhances the therapeutic potential of this platform by improving drug stability, controlling release kinetics, enhancing cellular uptake, promoting synergistic effects, enabling targeted delivery, reducing side effects, and facilitating combination therapy. These advantages make Nx-ZnO SNSs a promising platform for various biomedical applications, including drug delivery and therapeutics.

4. CONCLUSIONS

Chronic liver diseases present a substantial health burden on a global scale, and treatment options are limited. The potential hepatoprotective effects of ZnO nanomaterials stem from their regenerative, anti-inflammatory, and antioxidant characteristics. Nevertheless, their potential continues to be impeded by inadequate drug dosage and controlled release. In order to overcome these constraints, the present research investigates the intercalation of Nx, a highly effective analgesic and anti-inflammatory medication, within ZnO SNSs. A two-step solution phase easy approach was utilized herein to obtain Nx intercalated ZnO SNSs. The study employed various analytical techniques such as XRD, SEM, and FTIR spectroscopy to confirm the successful synthesis and intercalation of Nx within the ZnO SNSs. Our findings revealed that the stacking of ZnO SNSs was redistributed following adding Nx into highly ordered stacked arrangements. The obtained Nx-ZnO SNSs can be successfully encapsulated with PVA to make it more biocompatible. Furthermore, *in vivo* experiments using mice liver cells demonstrated the enhanced hepatoprotective potential of the Nx intercalated ZnO SNSs. Overall, the findings of this study provide valuable insights into the design and development of Nx intercalated ZnO SNSs as a promising platform for targeted drug delivery and enhanced therapeutic efficiency, specifically in the context of liver-related disorders. Overall, the findings of this study provide valuable insights into the design and development of Nx intercalated ZnO SNSs as a promising platform for targeted drug delivery and enhanced therapeutic efficiency, specifically in the context of liver-related disorders. Our newly developed solution-based strategy can be extended to obtain NSs of other types of materials. Moreover, various organic molecules, such as drugs, can be used as sheet stacking agents with self-incorporation into organic−inorganic hybrids. More biologically active materials with tunable properties can be achieved by proper selection of inorganic material, drug types, and surface modifiers polymers.

https://doi.org/10.1021/acsomega.4c02319
ACS Omega 2024, 9, 22979−22989

AUTHOR INFORMATION

Corresponding Authors

Bilal Akram − *Department of Chemistry, Tsinghua University, Beijing 100084, China; Department of Chemistry, Women University of Azad Jammu & Kashmir, Bagh 12500, Pakistan*; Email: bai-l16@tsinghua.org.cn

Bilal Ahmad Khan − *Department of Chemistry, The University of Azad Jammu & Kashmir, Muzaffarabad 13100, Pakistan*; orcid.org/0000-0002-7648-7359; Email: bkhan@ajku.edu.pk

Mahmoud A. A. Ibrahim − *Chemistry Department, Faculty of Science, Minia University, Minia 61519, Egypt; School of Health Sciences, University of KwaZulu-Natal, Durban 4000, South Africa*; orcid.org/0000-0003-4819-2040; Email: m.ibrahim@compchem.net

Authors

Muhammad Saleem Mughal − *Department of Chemistry, The University of Azad Jammu & Kashmir, Muzaffarabad 13100, Pakistan*

Tafail Akbar Mughal − *Department of Zoology, Women University of Azad Jammu & Kashmir, Bagh 12500, Pakistan*

Sulaiman Sulaiman − *Department of Chemistry, Islamia College University, Peshawar 25120, Pakistan*

Omar H. Abd-Elkader − *Department of Physics and Astronomy, College of Science, King Saud University, Riyadh 11451, Saudi Arabia*

Shaban R. M. Sayed − *Department of Botany and Microbiology, College of Science, King Saud University, Riyadh 11451, Saudi Arabia*

Ahmed M. Sidky − *Department of Neurology, The University of Chicago, Chicago, Illinois 60637-1476, United States; Chemistry Department, Faculty of Science, Minia University, Minia 61519, Egypt*

Complete contact information is available at: https://pubs.acs.org/10.1021/acsomega.4c02319

Author Contributions

M.S.M.: Data curation and methodology. B.A.: Data analysis and writing—original draft. B.A..K.: Conceptualization, methodology, project administration, resources, supervision, and writing—review and editing. T.A.M.: Data curation and methodology. S.S.: Formal analysis and writing—review and editing. O.A.-E.: Resources, formal analysis, and writing—original draft. S.R.M.S.: Resources and writing—review and editing. M.A.A. Ibrahim: Writing—review and editing. A.M.S.: Formal analysis and writing—review and editing.

Notes

The authors declare no competing financial interest.

Ethical Consideration The experiments were performed according to the approved protocol of the Ethical Committee on Animal Welfare of the Women University of Azad Jammu and Kashmir Bagh.

ACKNOWLEDGMENTS

The authors are grateful to the Researchers Supporting Project number (RSP2024R468), King Saud University, Riyadh, Saudi Arabia, for funding this work.

REFERENCES

(1) Akram, B.; Shi, W.; Zhang, H.; Ullah, S.; Khurram, M.; Wang, X. Free-standing CoO-POM janus-like ultrathin nanosheets. *Angew. Chem., Int. Ed.* **2020**, *59*, 8497−8501.

(2) Akram, B.; Wang, M.; Wang, X. PMA-FeCo mixed-oxide magnetic quasi-nanosheets. *Nanoscale* **2022**, *14*, 15635−15639.

(3) Akram, B.; Wang, X. Self-assembly of ultrathin nanocrystals to multidimensional superstructures. *Langmuir* **2019**, *35*, 10246−10266.

(4) Latif, S.; Akram, B.; Saraj, C. S.; Khan, B. A.; Ali, M.; Akhtar, J. A single step wet chemical approach to bifunctional ultrathin (ZnO)(62)(Fe(2)O(3))(38) dendritic nanosheets. *RSC Adv.* **2023**, *13*, 23038−23042.

(5) Li, Y.; Xia, Y.; Liu, K.; Ye, K.; Wang, Q.; Zhang, S.; Huang, Y.; Liu, H. Constructing Fe-MOF-derived Z-scheme photocatalysts with enhanced charge transport: Nanointerface and carbon sheath synergistic effect. *ACS Appl. Mater. Interfaces* **2020**, *12*, 25494−25502.

(6) Li, Y.; Liu, K.; Zhang, J.; Yang, J.; Huang, Y.; Tong, Y. Engineering the band-edge of Fe2O3/ZnO nanoplates via separate dual cation incorporation for efficient photocatalytic performance. *Ind. Eng. Chem. Res.* **2020**, *59*, 18865−18872.

(7) Liu, C.; Wang, B.; Han, T.; Shi, D.; Wang, G. Fe Foil-Guided Fabrication of Uniform Ag@AgX Nanowires for Sensitive Detection of Leukemia DNA. *ACS Appl. Mater. Interfaces* **2019**, *11*, 4820−4825.

(8) Jiang, M. W.; Han, T.; Zhang, X. J. Hollow C@SnS /SnS nanocomposites: High efficient oxygen evolution reaction catalysts. *J. Colloid Interface Sci.* **2021**, *583*, 149−156.

(9) Dai, T.; Wan, Y.; Tian, R.; Wang, S.; Han, T.; Wang, G. In situ cation exchange generated ZnS-Ag(2)S nanoparticles for photothermal detection of transcription factor. *ACS Appl. Bio Mater.* **2020**, *3*, 3260−3267.

(10) Novoselov, K. S.; Jiang, D.; Schedin, F.; Booth, T. J.; Khotkevich, V. V.; Morozov, S. V.; Geim, A. K. Two-dimensional atomic crystals. *Proc. Natl. Acad. Sci. U.S.A.* **2005**, *102*, 10451−10453.

(11) Zeng, Z.; Yin, Z.; Huang, X.; Li, H.; He, Q.; Lu, G.; Boey, F.; Zhang, H. Single-layer semiconducting nanosheets: high-yield preparation and device fabrication. *Angew. Chem., Int. Ed.* **2011**, *50*, 11093−11097.

(12) Coleman, J. N.; Lotya, M.; O'Neill, A.; Bergin, S. D.; King, P. J.; Khan, U.; Young, K.; Gaucher, A.; De, S.; Smith, R. J.; Shvets, I. V.; Arora, S. K.; Stanton, G.; Kim, H. Y.; Lee, K.; Kim, G. T.; Duesberg, G. S.; Hallam, T.; Boland, J. J.; Wang, J. J.; Donegan, J. F.; Grunlan, J. C.; Moriarty, G.; Shmeliov, A.; Nicholls, R. J.; Perkins, J. M.; Grieveson, E. M.; Theuwissen, K.; McComb, D. W.; Nellist, P. D.; Nicolosi, V. Two-dimensional nanosheets produced by liquid exfoliation of layered materials. *Science* **2011**, *331*, 568−571.

(13) Zhou, K. G.; Mao, N. N.; Wang, H. X.; Peng, Y.; Zhang, H. L. A mixed-solvent strategy for efficient exfoliation of inorganic graphene analogues. *Angew. Chem., Int. Ed.* **2011**, *50*, 10839−10842.

(14) Zhang, H. T.; Savitzky, B. H.; Yang, J.; Newman, J. T.; Perez, K. A.; Hyun, B. R.; Kourkoutis, L. F.; Hanrath, T.; Wise, F. W. Colloidal synthesis of PbS and PbS/CdS nanosheets using acetate-free precursors. *Chem. Mater.* **2016**, *28*, 127−134.

(15) Liu, K. K.; Zhang, W.; Lee, Y. H.; Lin, Y. C.; Chang, M. T.; Su, C. Y.; Chang, C. S.; Li, H.; Shi, Y.; Zhang, H.; Lai, C. S.; Li, L. J. Growth of large-area and highly crystalline MoS2 thin layers on insulating substrates. *Nano Lett.* **2012**, *12*, 1538−1544.

(16) Kaneti, Y. V.; Salunkhe, R. R.; Septiani, N. L. W.; Young, C.; Jiang, X. C.; He, Y. B.; Kang, Y. M.; Sugahara, Y.; Yamauchi, Y. General template-free strategy for fabricating mesoporous two-dimensional mixed oxide nanosheets self-deconstruction/reconstruction of monodispersed metal glycerate nanospheres. *J. Mater. Chem. A* **2018**, *6*, 5971−5983, DOI: 10.1039/C8TA00008E.

(17) Akram, B.; Ali, M.; Liu, Q. D. Polyoxometalate induced assembly into surface functionalized multidimensional heterostructures with enhanced catalytic activity. *Small Methods* **2024**, No. 2301432.

(18) Zhang, L.; Feng, K. C.; Yu, Y.; Chuang, Y. C.; Chang, C. C.; Vadada, S.; Patel, R.; Singh, V.; Simon, M.; Rafailovich, M. Effect of graphene on differentiation and mineralization of dental pulp stem

cells in poly(4-vinylpyridine) matrix in vitro. *ACS Appl. Bio Mater.* **2019**, *2*, 2435−2443.
(19) Li, Y.; Wang, J.; Tang, Y.; Lu, S.; Lv, Y.; Li, W.; Zhang, M.; Yu, Y. Stimuli-responsive ultra-small vanadate prodrug nanoparticles with NIR photothermal properties to precisely inhibit Na/K-ATPase for enhanced cancer therapy. *Nanoscale* **2023**, *15*, 9116−9122.
(20) Kanwal, N.; Akram, B.; Saraj, C. S.; Ahmad, K.; Talib, S. H.; Asif, H. M. Counterion-controlled synthesis of multifunctional iron cobalt mixed oxide laminar superstructures. *New J. Chem.* **2022**, *46*, 9762−9766.
(21) Akram, B.; Ahmad, K.; Khan, J.; Khan, B. A.; Akhtar, J. Low-temperature solution-phase route to sub-10 nm titanium oxide nanocrystals having super-enhanced photoreactivity. *New J. Chem.* **2018**, *42*, 10947−10952.
(22) Chen, S. J.; Liu, Y. C.; Shao, C. L.; Mu, R.; Lu, Y. M.; Zhang, J. Y.; Shen, D. Z.; Fan, X. W. Structural and optical properties of uniform ZnO nanosheets. *Adv. Mater.* **2005**, *17*, 586−590.
(23) Khan, H. R.; Akram, B.; Aamir, M.; Malik, M. A.; Tahir, A. A.; Choudhary, M. A.; Akhtar, J. Fabrication of Mn−ZnO photoanodes for photoelectrochemical water splitting applications. *J. Mater. Sci.: Mater. Electron.* **2021**, *32*, 20946−20954.
(24) Hafeez, M.; Arshad, R.; Hameed, M. U.; Akram, B.; Ahmed, M. N.; Kazmi, S. A.; Ahmad, I.; Ali, S. *Populus ciliata* leaves extract mediated synthesis of zinc oxide nanoparticles and investigation of their anti-bacterial activities. *Mater. Res. Express* **2019**, *6*, No. 075064, DOI: 10.1088/2053-1591/ab19c8.
(25) Bains, D.; Singh, G.; Singh, N. Sustainable synthesis of ionic liquid-functionalized zinc oxide nanosheets (IL@ZnO): Evaluation of antibacterial potential activity for biomedical applications. *ACS Appl. Bio Mater.* **2022**, *5*, 1239−1251.
(26) Zabihi, E.; Babaei, A.; Shahrampour, D.; Arab-Bafrani, Z.; Mirshahidi, K. S.; Majidi, H. J. Facile and rapid in-situ synthesis of chitosan-ZnO nano-hybrids applicable in medical purposes; a novel combination of biomineralization, ultrasound, and bio-safe morphology-conducting agent. *Int. J. Biol. Macromol.* **2019**, *131*, 107−116.
(27) Islam, F.; Shohag, S.; Uddin, M. J.; Islam, M. R.; Nafady, M. H.; Akter, A.; Mitra, S.; Roy, A.; Bin Emran, T.; Cavalu, S. Exploring the journey of zinc oxide nanoparticles (ZnO-NPs) toward biomedical applications. *Materials* **2022**, *15*, No. 2160, DOI: 10.3390/ma15062160.
(28) Zhang, Y.; Nayak, T. R.; Hong, H.; Cai, W. Biomedical applications of zinc oxide nanomaterials. *Curr. Mol. Med.* **2013**, *13*, 1633−1645.
(29) Fouda, A.; El-Din Hassan, S.; Salem, S. S.; Shaheen, T. I. In-Vitro cytotoxicity, antibacterial, and UV protection properties of the biosynthesized Zinc oxide nanoparticles for medical textile applications. *Microb. Pathog.* **2018**, *125*, 252−261.
(30) Youn, S. M.; Choi, S. J. Food additive zinc oxide nanoparticles: Dissolution, interaction, fate, cytotoxicity, and oral toxicity. *Int. J. Mol. Sci.* **2022**, *23*, No. 6074, DOI: 10.3390/ijms23116074.
(31) Buerki-Thurnherr, T.; Xiao, L.; Diener, L.; Arslan, O.; Hirsch, C.; Maeder-Althaus, X.; Grieder, K.; Wampfler, B.; Mathur, S.; Wick, P.; Krug, H. F. In vitro mechanistic study towards a better understanding of ZnO nanoparticle toxicity. *Nanotoxicology* **2013**, *7*, 402−416.
(32) Ma, H.; Williams, P. L.; Diamond, S. A. Ecotoxicity of manufactured ZnO nanoparticles–a review. *Environ. Pollut.* **2013**, *172*, 76−85.
(33) Xie, J. N.; Li, H. L.; Zhang, T. R.; Song, B. K.; Wang, X. H.; Gu, Z. J. Recent advances in ZnO nanomaterial-mediated biological applications and action mechanisms. *Nanomaterials* **2023**, *13*, No. 1500, DOI: 10.3390/nano13091500.
(34) Hong, T. K.; Tripathy, N.; Son, H. J.; Ha, K. T.; Jeong, H. S.; Hahn, Y. B. A comprehensive in vitro and in vivo study of ZnO nanoparticles toxicity. *J. Mater. Chem. B* **2013**, *1*, 2985−2992.
(35) Kamali Shahri, S. M.; Sharifi, S.; Mahmoudi, M. Interdependency of influential parameters in therapeutic nanomedicine. *Expert Opin. Drug Delivery* **2021**, *18*, 1379−1394.
(36) Colombo, M.; Carregal-Romero, S.; Casula, M. F.; Gutiérrez, L.; Morales, M. P.; Böhm, I. B.; Heverhagen, J. T.; Prosperi, D.; Parak, W. J. Biological applications of magnetic nanoparticles. *Chem. Soc. Rev.* **2012**, *41*, 4306−4334.
(37) Lee, S.; Stubelius, A.; Hamelmann, N.; Tran, V.; Almutairi, A. Inflammation-responsive drug-conjugated dextran nanoparticles enhance anti-inflammatory drug efficacy. *ACS Appl. Mater. Interfaces* **2018**, *10*, 40378−40387.
(38) Zhang, L. Z.; Li, G. C.; Gao, M.; Liu, X.; Ji, B.; Hua, R. H.; Zhou, Y. L.; Yang, Y. M. RGD-peptide conjugated inulin-ibuprofen nanoparticles for targeted delivery of Epirubicin. *Colloids Surf., B* **2016**, *144*, 81−89.
(39) Davies, N. M.; Anderson, K. E. Clinical pharmacokinetics of naproxen. *Clin. Pharmacokinet.* **1997**, *32*, 268−293.
(40) Datta, S.; Aggarwal, D.; Sehrawat, N.; Yadav, M.; Sharma, V.; Sharma, A.; Zghair, A. N.; Dhama, K.; Sharma, A.; Kumar, V.; Sharma, A. K.; Wang, H. Hepatoprotective effects of natural drugs: Current trends, scope, relevance and future perspectives. *Phytomedicine* **2023**, *121*, No. 155100.
(41) Jayakumar, A.; Radoor, S.; Nair, I. C.; Siengchin, S.; Parameswaranpillai, J.; Radhakrishnan, E. K. Lipopeptide and zinc oxide nanoparticles blended polyvinyl alcohol-based nanocomposite films as antimicrobial coating for biomedical applications. *Process Biochem.* **2021**, *102*, 220−228.
(42) Chakraborti, S.; Joshi, P.; Chakravarty, D.; Shanker, V.; Ansari, Z. A.; Singh, S. P.; Chakrabarti, P. Interaction of polyethyleneimine-functionalized ZnO nanoparticles with bovine serum albumin. *Langmuir* **2012**, *28*, 11142−11152.
(43) Bhadra, P.; Mitra, M. K.; Das, G. C.; Dey, R.; Mukherjee, S. Interaction of chitosan capped ZnO nanorods with. *Mater. Sci. Eng., C* **2011**, *31*, 929−937.
(44) Schulze, F.; Dienelt, A.; Geissler, S.; Zaslansky, P.; Schoon, J.; Henzler, K.; Guttmann, P.; Gramoun, A.; Crowe, L. A.; Maurizi, L.; Vallee, J. P.; Hofmann, H.; Duda, G. N.; Ode, A. Amino-polyvinyl alcohol coated superparamagnetic iron oxide nanoparticles are suitable for monitoring of human mesenchymal stromal cells in vivo. *Small* **2014**, *10*, 4340−4351.
(45) Ebadi, M.; Bullo, S.; Buskara, K.; Hussein, M. Z.; Fakurazi, S.; Pastorin, G. Release of a liver anticancer drug, sorafenib from its PVA/LDH- and PEG/LDH-coated iron oxide nanoparticles for drug delivery applications. *Sci. Rep.* **2020**, *10*, No. 21521.
(46) Pulit-Prociak, J.; Staron, A.; Prokopowicz, M.; Magielska, K.; Banach, M. Analysis of antimicrobial properties of PVA-based coatings with silver and zinc oxide nanoparticles. *J. Inorg. Organomet. Polym. Mater.* **2021**, *31*, 2306−2318.
(47) Mughal, T. A.; Saleem, M. Z.; Ali, S.; Anwar, K. K.; Bashiri, M. M.; Babar, M.; Khan, M. A. Evaluation of hepatotoxicity of carbon tetrachloride and pharmacological intervention by vitamin e in Balb C mice. *Pak. J. Zool.* **2019**, *51*, 755−761.
(48) Tanak, H.; Ersahin, F.; Köysal, Y.; Agar, E.; Isik, S.; Yavuz, M. Theoretical modeling and experimental studies on N-n-Decyl-2-oxo-5-nitro-1-benzylidene-methylamine. *J. Mol. Model.* **2009**, *15*, 1281−1290.
(49) Saji, R. S.; Prasana, J. C.; Muthu, S.; George, J.; Kuruvilla, T. K.; Raajaraman, B. R. Spectroscopic and quantum computational study on naproxen sodium. *Spectrochim. Acta, Part A* **2020**, *226*, No. 117614.
(50) Zhong, Z. Y.; Karin, M. NF-kB restricts inflammasome activation via elimination of damaged mitochondria. *Cancer Immunol. Res.* **2016**, *4*, 896−910, DOI: 10.1016/j.cell.2015.12.057.
(51) Palaniyappan, N.; Subramanian, V.; Ramappa, V.; Ryder, S. D.; Kaye, P.; Aithal, G. P. The utility of scoring systems in predicting early and late mortality in alcoholic hepatitis: Whose score is it anyway? *Int. J. Hepatol.* **2012**, *2012*, 1−5.
(52) Abel, S.; Gelderblom, W. C. Oxidative damage and fumonisin B1-induced toxicity in primary rat hepatocytes and rat liver in vivo. *Toxicology* **1998**, *131*, 121−131.
(53) Hong, Z. F.; Zhao, W. X.; Yin, Z. Y.; Xie, C. R.; Xu, Y. P.; Chi, X. Q.; Zhang, S.; Wang, X. M. Capsaicin enhances the drug sensitivity

of cholangiocarcinoma through the inhibition of chemotherapeutic-induced autophagy. *PLoS One* **2015**, *10*, No. e0121538.
(54) Salem, M. B.; Affes, H.; Ksouda, K.; Dhouibi, R.; Sahnoun, Z.; Hammami, S.; Zeghal, K. M. Pharmacological studies of artichoke leaf extract and their health benefits. *Plant Foods Hum. Nutr.* **2015**, *70*, 441−453.
(55) Madrigal-Santillán, E. Review of natural products with hepatoprotective effects. *World J. Gastroenterol.* **2014**, *20*, 14787.
(56) Ritesh, K. R.; Suganya, A.; Dileepkumar, H. V.; Rajashekar, Y.; Shivanandappa, T. A single acute hepatotoxic dose of CCl(4) causes oxidative stress in the rat brain. *Toxicol. Rep.* **2015**, *2*, 891−895.
(57) Ramappa, V.; Aithal, G. P. Hepatotoxicity related to anti-tuberculosis drugs: Mechanisms and management. *J. Clin. Exp. Hepatol.* **2013**, *3*, 37−49.
(58) Williams, G. M.; Iatropoulos, M. J. Alteration of liver cell function and proliferation: Differentiation between adaptation and toxicity. *Toxicol. Pathol.* **2002**, *30*, 41−53.
(59) Jaeschke, H.; McGill, M. R.; Ramachandran, A. Oxidant stress, mitochondria, and cell death mechanisms in drug-induced liver injury: lessons learned from acetaminophen hepatotoxicity. *Drug Metab. Rev.* **2012**, *44*, 88−106.
(60) Benahmed, F.; Rached, W.; Kerroum, F.; Zohra Belhouari, H. F.; Mehrab, E. a.; Talhi, H.; Belmokhtar, M.; Kharoubi, O. Protective effect of Pistacia atlantica Desf leaves on Mercury-Induced toxicity in Rats. *South Asian J. Exp. Biol.* **2020**, *10*, 152−161, DOI: 10.38150/sajeb.10(3).

https://doi.org/10.1021/acsomega.4c02319
ACS Omega 2024, 9, 22979−22989